HORIZON EUROPE PROGRAMME
HORIZON-CL4-2023-DIGITAL-EMERGING-01-33

GA No. 101135196

Developing New 2D Materials and Heterostructures for Printed Digital Devices

2D-PRINTABLE - Deliverable report

D4.3 – Protocols for new characterization methodologies

Funded by
the European Union

Deliverable No.	D4.3	
Related WP	WP4	
Deliverable Title	Protocols for new characterization methodologies	
Deliverable Date	30/09/2025	
Deliverable Type	REPORT	
Dissemination level	Public (PU)	
Author(s)	Cian Gabbett (TCD) Tim Nowack (Uka)	20/09/2025
Checked by	Jonathan Coleman (TCD)	30/09/2025
Reviewed by	Claudia Backes (UKa) Ali Shaygan Nia (TUD)	30/09/2025
Approved by	Jonathan Coleman (TCD) - Project Coordinator	30/09/2025
Status	Draft v2	30/09/2025

Document History

Version	Date	Editing done by	Remarks
V1.0	28/09/2025	Cian Gabbett & Tim Nowack	
V2.0	30/09/2025	Claudia Backes	
V2.1			
FINAL			

Project Scientific Abstract

The 2D-PRINTABLE project aims to integrate sustainable large-scale liquid exfoliation techniques with theoretical modelling to efficiently produce a wide range of new 2D materials (2DMs), including conducting, semiconducting, and insulating nanosheets. The focus includes developing the printing and liquid phase deposition methods required to fabricate networks and multicomponent heterostructure/s, featuring layer-by-layer assembly of nanometer-thick 2DMs into ordered multilayers. The goal is to optimize these printed networks and heterostructures for digital systems, unlocking new properties and functionalities. The project also seeks to demonstrate various printed digital devices, including proof-of-principle, first-time demonstration of all-printed, all-nanosheet, heterostack light-emitting diodes (LEDs). In conclusion, 2D-PRINTABLE will prove 2D materials to be an indispensable material class in the field of printed electronics, capable of producing far-beyond-state-of-the-art devices that can act as a platform for the next generation of printed digital applications.

Public summary

This deliverable reports on the development of two complementary characterisation methodologies for 2D materials and their networks: diffuse reflectance infrared Fourier transform (DRIFT) spectroscopy and focused ion beam-scanning electron microscopy nanotomography (FIB-SEM NT).

Within 2D-PRINTABLE, DRIFT spectroscopy has been established as a protocol for probing the chemical cleanliness of 2D nanosheets using liquid phase exfoliated (LPE) MoS_2 nanosheets as a model system. During exfoliation and processing, surfactants, solvents, or other additives are often introduced to stabilise 2DM dispersions. However, these molecules can remain bound to nanosheet surfaces. If not removed, they can act as dopants, scattering centres, increase the resistance at inter-flake junctions (R_J), or can hinder further functionalisation. DRIFT spectroscopy is uniquely sensitive to the vibrational fingerprints of organic molecules and surfactants in the mid- and far-infrared range. By mixing nanosheets with an infrared-transparent matrix, this method enables detection and comparison of even small amounts of residues on 2D materials such as MoS_2. Establishing this capability is crucial, as nanosheet cleanliness at the chemical level directly impacts how reliably they can be functionalised or assembled into networks and devices.

In contrast, FIB-SEM nanotomography was used to address the structural side of 2DM network optimisation by reconstructing their morphology in 3D with nanometre resolution. Protocols to extract quantitative measurements of network porosity, tortuosity, nanosheet alignment, and interfacial roughness have been developed as part of D4.3. This is demonstrated by comparing the structure of printed graphene networks made up of LPE and electrochemically exfoliated (EE) nanosheets. Here, the EE graphene networks were found to be significantly denser and more well-connected and aligned than their LPE counterparts, which can be linked to their vastly superior charge transport properties.

Together, the two protocols provide a dual approach: DRIFT spectroscopy establishes the cleanliness of the nanosheets, while FIB-SEM NT quantifies the morphology of the networks they form. This strategy now provides the consortium with validated methods to link nanosheet quality to network architecture, enabling the design of cleaner, more well-connected 2DM networks for high-performance printed devices.

Contents

List of Figures

Abbreviations & Definitions

Abbreviation	Explanation
2DM	Two-dimensional Materials
EE	Electrochemical Exfoliation
LPE	Liquid Phase Exfoliation
FIB-SEM NT	Focused Ion Beam - Scanning Electron Microscope Nanotomography
LED	Light Emitting Diode
TFT	Thin Film Transistor
DRIFTS	Diffuse Reflectance Infrared Fourier Transform Spectroscopy
MIR	Mid-Infrared
FIR	Far-Infrared
UV-Vis Spectroscopy	Ultraviolet-Visible Spectroscopy
XPS	X-ray Photoelectron Spectroscopy
ATR	Attenuated Total Reflection

1 Introduction

This report outlines the development of new characterisation protocols to address two central bottlenecks in printed two-dimensional material (2DM) networks and devices: nanosheet cleanliness and network morphology. At the nanoscale, residual solvents, surfactants, or additives can persist on the nanosheet surface after solution-phase processing. These molecules can act as dopants or scattering centres, increasing the inter-flake junction resistance (R_J) and limiting charge transport in devices. In addition, such residues inhibit further functionalisation of the nanosheets, restricting opportunities for controlled chemical modification or integration into heterostructures. To address this, protocols for diffuse reflectance infrared Fourier transform (DRIFT) spectroscopy were developed using LPE MoS_2 as a model 2DM system. These procedures allow reproducible detection and analysis of organics and additives across mid- and far-infrared ranges in both dispersions and powders. This establishes a route towards benchmarking nanosheet cleanliness and functionalisation potential, as well as informing improved cleaning protocols. A first publication is in review.

At the 2DM network level, device performance is strongly controlled by the way that the nanosheets assemble. Porosity, nanosheet alignment, tortuosity, and interfacial roughness determine whether networks are well connected or dominated by high-resistance junctions. To quantify these parameters, protocols for focused ion beam-scanning electron microscopy nanotomography (FIB-SEM NT) were developed and applied to printed graphene networks. Volumetric reconstructions at nanometre resolution provided direct comparison between liquid-phase exfoliated (LPE) and electrochemically exfoliated (EE) graphene films, showing EE films to be far denser and more well-connected than their LPE counterparts. These findings validate FIB-SEM NT as a powerful tool for benchmarking 2DM network morphology and have been disseminated in several peer-reviewed publications acknowledging 2D-PRINTABLE[1-3].

Together, the DRIFT spectroscopy and FIB-SEM NT methodologies provide complementary information on nanosheet chemistry and network structure. This combined approach enables a systematic route to producing cleaner nanosheets and depositing optimised networks and devices, establishing a foundation for improved charge transport and reproducible device fabrication across the 2D-PRINTABLE project.

2 Methods

2.1 Background

As part of Deliverable 4.3, methodologies to characterise both nanosheets and their nanostructured devices were developed and optimised. The performance of printed 2D material (2DM) networks and heterostructures is determined by two interconnected factors; the cleanliness of the nanosheets themselves and the morphology of the networks/devices into which they are assembled. Residual additives, surfactants, or solvents left on nanosheet surfaces can act as dopants, scatterers, or barriers to van der Waals coupling. This can increase the inter-nanosheet junction resistance, R_J, which has a deleterious effect on interflake charge transport and ultimately reduces device performance. At the same time, poorly optimised nanosheet stacking in printed 2DM networks leads to high junction resistances, porous morphologies, and rough interfaces, all of which degrade charge transport and stability in printed devices. To address these challenges, two complementary characterisation protocols were developed and their methodologies are described in this report. DRIFT spectroscopy provides a sensitive probe of organics and additives on nanosheet surfaces, enabling both quantitative and qualitative analysis of residues at mid- and far-infrared frequencies. In parallel, FIB-SEM nanotomography was used to reconstruct printed 2DM networks and devices at nanometre resolution, delivering quantitative metrics such as porosity, tortuosity, nanosheet alignment, and surface roughness. Together, these methodologies facilitate complementary information on both the nanosheet quality and network/device morphology - two key parameters that must be optimised to form state-of-the-art printed 2DM devices. The protocols developed as part of D4.3 aim to provide a clear route towards producing cleaner nanosheets and optimised network structures with improved interfaces and charge transport properties.

2.2 Procedures

2.2.1 DRIFT Spectroscopy

To prepare MoS_2 samples for DRIFT spectroscopy two procedures were followed, depending on whether the starting material was in solution or in powder form. MoS_2 2DM inks were prepared using liquid phase exfoliation[4] (as described e.g. in D3.1) and centrifuged at 30k *g* in 1.5 mL Eppendorf SafeLock tubes using a Hettich Mikro 220R centrifuge. The sediment was retained and redispersed in fresh DI water. For the smallest fraction, Beckman Coulter 1.5 mL polypropylene tubes and an Avanti J-26 XP centrifuge were used at 21 krpm (JA-25.50 rotor with the necessary adapters). The obtained aqueous dispersions were then frozen in liquid nitrogen and freeze-dried in a Zirbus VaCo 2 at 0.1 mbar for 24 h. The obtained powder from this step was treated as discussed below.

For 2DM powders the following protocol was applied, unless otherwise stated in the discussion section. The obtained powders (~ 0.5 - 1 mg) were mixed with CsI (~ 100 mg, ThermoFisher 10022) in an agate mortar and then transferred to the microbeakers of a PerkinElmer Spectrum 3 FTIR spectrometer equipped with a diffuse reflectance sampling accessory. The autofocus function was used for a background measurement using a microbeaker with pure CsI, with the same procedure for sample measurements. Automatic CO_2/H_2O correction was done in the mid-infrared (MIR) region. At

least 50 and 100 spectra were collected and averaged in the MIR and far-infrared (FIR) respectively. Spectra were acquired in 1 cm^{-1} increments (achieved by setting the internal resolution to 4 cm^{-1}) and a scan speed of 0.2 cm s^{-1} was used. After Kubelka-Munk transformation and manual baseline subtraction, MoS_2 related spectra were normalized to the shear mode of MoS_2 at 384 cm^{-1}.

2.2.2 FIB-SEM Nanotomography

FIB-SEM NT was performed using a dual-beam Carl ZEISS Auriga system. ZEISS ATLAS 5 software was used for the nanotomography process, where hundreds of sequential network cross-sections were milled and imaged. A pixel size of 5 nm and a slice thickness of 15 nm were used for each cross section across all samples, giving a voxel size of 5 × 5 × 15 nm. All cross-sections were milled using a 600 pA beam and imaged under standardised conditions (30 µm aperture, 5 mm working distance and a 2 kV accelerating voltage) using both the Inlens and SE2 detectors. The greyscale SEM images were classified into the discrete phases (i.e. nanosheet, pore, substrate) using trainable machine learning via the Trainable WEKA Segmentation[5] plugin in FIJI[6]. The result of the classification process was image stacks that contained only information on a chosen phase, such as the nanosheets. These stacks were then aligned and interpolated to from a 3D reconstruction of the nanosheet network using Dragonfly (Object Research Systems). To extract quantitative information from these 3D images, a variety of protocols were developed. The network porosity was calculated using the Taufactor[7] application in MATLAB. The connectivity of a given phase in the 2DM networks and devices was also calculated in Taufactor by measuring its tortuosity factor in the *x*-, *y*-, and *z*-directions. Protocols to analyse the nanosheet alignment both within the 2DM networks and at their surfaces/interfaces were also developed. The bulk nanosheet alignment within each network was found by isolating discrete nanosheets in the 3D images using a 3D Distance Transform Watershed within the MorpholibJ[8] plugin in FIJI. The polar angle, ϕ_{NS}, between the normal vector describing each nanosheet, $\hat{n}$, and the *y*-axis direction (perpendicular to the substrate in the out-of-plane direction) was then measured in FIJI.

Data Analysis

Data analysis was performed using specialised software specific to each technique as needed. OriginPro was used for generalised numerical and statistical analysis, curve fitting and production of graphs. For the FIB-SEM NT generated network volumes, both the porosity and tortuosity factor were measured using the Taufactor application in MATLAB[7]. Individual nanosheets inside the 2DM networks were identified from 3D images using a 3D Distance Transform Watershed within the MorpholibJ[8] plugin in FIJI. Surface gradient maps and network roughness metrics were generated in MATLAB.

3 Results & Discussion

3.1 Results

3.1.1 DRIFT Spectroscopy of MoS_2 Nanosheets

a) *Why use DRIFT spectroscopy in the context of liquid-processed nanomaterials?*

In modern nanomaterial-based device fabrication, liquid processing plays an important role[9]. However, the utilised solvent/additive molecules can remain on the newly created nano-surfaces. This poses a particular problem for 2DMs from a chemical perspective, as residual organic molecules from solution processing can hinder or interfere with further controlled surface modification, such as functionalization reactions (see for example D2.1). From a physical perspective, these molecules can induce doping and other undesired effects on the performance of the 2DMs in electrical devices[10,11] and present a barrier in the fabrication of heterostructures with atomically-clean van der Waals contacts between the nanosheets. In this work, MoS_2 was used as a model compound for analysis.

From the broad range of available characterization techniques in this field, the established procedures to probe chemical material modification are absorption and emission spectroscopy (typically in the UV-Vis range), Raman and X-ray photoelectron spectroscopy (XPS). UV-Vis spectroscopy requires potential electronic transitions of the specimen in the UV-visible range. Here, spectra are dominated by 2DM related transitions[12], while common solvents like H_2O or NMP appear with different cut-off wavelengths in the UV region. Bands related to ink additives are usually only reported in cases where 2DM functionalization with a photoactive molecule was the target of the experiment[13]. Further, surface adsorbates can result in quenching and shifts of excitonic transitions due to chemical doping,[14] giving some indirect observable in comparative studies. Raman spectroscopy is a widely applied to both solid and liquid 2DM samples and can reveal information about crystal polymorphs, layer number or defects[15]. However, the resonance Raman effect of MoS_2 upon visible excitation, which is necessary to extract the above information, also obscures the intrinsic vibrational modes of any additives present. XPS can provide information on the elemental composition of each specimen and via exact binding energies and the contributions of chemically different species also information about oxidation states and hence, defects, functionalization or doping. However, discrete information on chemical bonds can only be obtained reconstructively (or indirectly).

Supplementing these methods with a vibrational spectroscopy technique that is more sensitive to organic impurities (relative to the MoS_2 host) would be highly valuable. IR spectroscopy is a technique that potentially fulfils these requirements, while also being relatively low-cost to implement and commonly available in many chemical laboratories as it is an established technique for characterizing organic molecules. A further benefit is the availability of large databases of molecular spectra. The tag "organic" already highlights why most spectrometers are optimized for measurements in the mid-infrared range (400 - 4000 cm^{-1}), where carbon-based vibrations are expected. This means that optical windows, internal light guides and analyte matrix materials are optimised for this range. If the aim is to analyse vibrations of MoS_2 in addition to the organic residues, it should be highlighted that the

intrinsic MoS_2 modes can typically be found around 467 and 384 cm^{-1}, which is at the edge of the far-infrared region[16]. Transmission-based IR measurements are possible in this range when the optical windows, beam splitters and matrix material (from KBr to CsI) are adapted. Solid state spectra in transmission can be obtained from pressed discs of these powders. These often suffer from residual water content in the sample, which hinders characterization due to overlapping signals and additional interactions. For this reason, many laboratories have changed their standard setup towards Attenuated Total Reflection (ATR) infrared spectroscopy, where no additional matrix powder or disc pressing is necessary. This method, however, requires a higher refractive index for the ATR element compared to the analyte, as well as transparency of the ATR element to the wavelengths used for analysis. For the chosen model compound MoS_2 and related 2DM, the refractive index in the FIR poses a problem[17-19]. Therefore, in this work, Diffuse Reflectance Infrared Fourier Transformation (DRIFT) spectroscopy will be used.

b) *DRIFT Spectroscopy Setup & Spectral Interpretation*

In the diffuse reflectance accessory, the light beam is focused onto the material and the diffusely scattered light is collected and guided to the detector. It should be noted, that diffuse reflectance spectra are typically not shown in % transmission units, but typically rather on scales of log(1/*R*), where *R* is the reflectance, or Kubelka-Munk units[20]. The former represents a simple mathematical transformation analogous to the transmission/absorption transformation in common extinction (UV-VIS) spectroscopy, while the latter represents a model derived to truly account for diffuse scattering and absorption events of the incident beam at powder surfaces. It assumes specifics for sample preparation such as constant scattering coefficient and infinite sample dilution in a non-absorbing matrix[21]. Furthermore, it is assumed that no light is transmitted (i.e. the sample is infinitely thick), which is typically satisfied in standard holders for sample thicknesses of 3 - 5 mm[22]. This is achieved by grinding the analyte (MoS_2) powder with CsI as the matrix material (mass ratio $\sim$ 1:100) to comparable particle sizes in an agate mortar. A ground sample of CsI is used for the background measurement. The reflectance signal measured (here R_∞; the index indicates an “infinitely” thick sample) is transformed into Kubelka-Munk units according to the following equation:

$$\frac{k}{s} = \frac{(1-R_\infty)^2}{2R_\infty} \qquad \text{Eqn. 1}$$

where k represents the absorption coefficient and s the scattering coefficient. Assuming a broadly constant scattering coefficient within the model, this expression should deliver information proportional to the sample absorption and thus also the concentration. However, to fulfill this assumption, extreme care must be taken during sample preparation to ensure comparable particle sizes and an appropriate refractive index of the sample (which can be affected by the mixing ratio of analyte and matrix) or packing density of the powder. Even though these requirements appear challenging and literature discussions about adequate evaluation of reflectance measurements are ongoing[23], the Kubelka-Munk transformation of signals will be applied here to identify qualitative and/or relative changes in recorded spectra. Further information on the derivation of the model can be found in the literature[22,24-26]. To demonstrate this approach, we will **c)** illustrate the stepwise processing of reflection data towards a baseline-corrected Kubelka-Munk spectrum, and **d)** outline initial optimization of sample preparation.

***c)** Spectral correction and Kubelka-Munk transformation*

The initial DRIFT spectrum obtained is plotted in % transmission values relative to the signal obtained from the background measurement (Fig. 1a). Depending on the exact mixing ratio of sample/analyte and whether the micro beaker was filled with the powder in a comparable way (filling height, equally even powder surfaces, etc.) values slightly above 100 % transmission were observed in some cases. Direct transformation to Kubelka-Munk units would level ranges around these peaks to linear shapes, which is why an interactive baseline correction (flat line subtraction; black to red trace in Fig. 1a) is employed to manually set the highest value to 100 % transmission prior to Kubelka-Munk transformation (red trace in Fig. 1a to green trace in Fig. 1b). Following this, a manual baseline subtraction is performed. The baseline shape roughly follows an exponential and should retain the clear features around 3500 cm^{-1} for O-H bands and around 2900 cm^{-1} for C-H bands, while subtracting the background in the region 1700-2800 cm^{-1} which we found bereft of features.

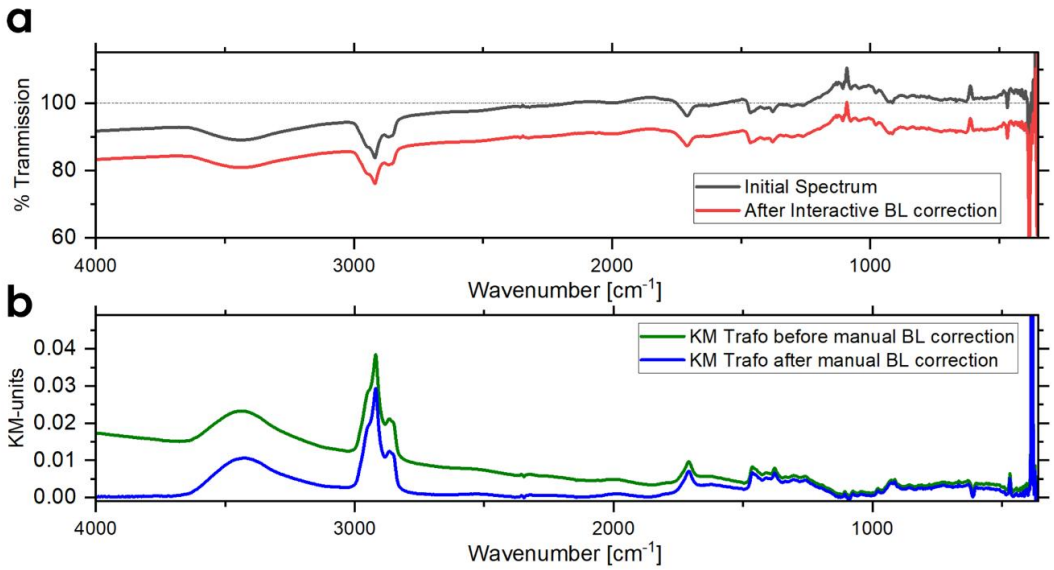

***Figure 1: Steps of DRIFT spectroscopy data processing. a)** Interactive Baseline Correction to avoid loss of spectral data during Kubelka Munk Transformation (Trafo)resulting in a transformation of the black to red curve. This red curve is then transformed to the green curve in **b)** using the Kubelka-Munk Transformation. **b)** Manual baseline correction applied to the green curve to correct resulting in the final spectrum (blue line). A specimen of LPE MoS_2 ($<N>_{vf}$ = 9) after freeze-drying and mixing with CsI was used and the measurement was performed in micro beakers.*

***d)** Evaluation of sample preparation*

The most common sample holders for DRIFT spectroscopy are either micro beakers which are commonly used for powders, or abrasive pads or abrasive sticks that can be utilised to remove analyte material from hard substances (Fig. 2). Initial experiments as part of D4.3 focused on MoS_2 powders, which were hard to reproducibly distribute on abrasive sticks. For this reason, abrasive sticks were excluded from

***Figure 2: DRIFT sample holders.** Left: abrasive pad, right: microbeaker. Inset shows powder applied to the abrasive pad. The micro beaker is shown with powders of MoS_2 mixed with CsI as matrix material.*

the following results. However, both other options were tested using commercial MoS_2. Results are compared in Figure 3 with data processing as explained in **(c)**. The vibrational modes of MoS_2 can be observed in all cases. The range between 1800-2700 cm^{-1} is not displayed due to the absence of any modes in either of the methods/samples. The broad features around 1150, 1450 and 3230 cm^{-1} which can only be seen in pad-based spectra can in principle stem from impurities in the MoS_2 powder. However, they are not observed in the microbeaker spectra so that it is more likely that they are caused by background (substrate) effects (e.g. inhomogeneous coverage of the pad) and/or different water contents in the samples, as OH-based vibrations can potentially be found in this spectral ranges. As also some vibrations are observed in the microbeaker spectra, this highlights the necessity of dry matrix materials. As it generally appears more reproducible during this work, the micro-beaker method will be further pursued and discussed.

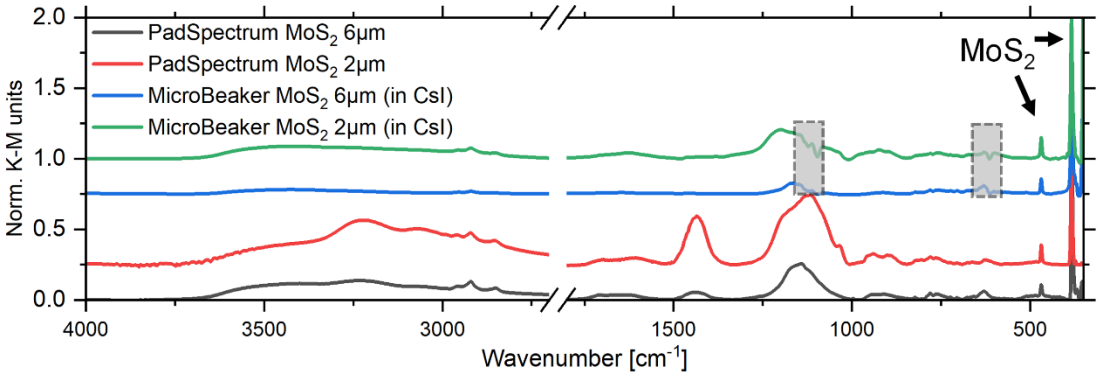

Figure 3: DRIFT Spectra of MoS_2 Powders. *DRIFT spectra in the mid infrared of commercially available MoS_2 powders (both Sigma Aldrich, particle size 6 µm corresponds to # 69860-100g; 2 µm corresponds to #234842-100g). To facilitate comparison all spectra were normalized to the in-plane MoS vibration around 384 cm^{-1}. Distributed powder on reflective pad was compared to measurements in micro beakers after mixing and grinding with CsI. Grey boxes indicate background related signals from CsI-matrix.*

Another benefit of utilising matrix materials for mixing with the analyte is the reduced material mass that is required: especially for powders obtained from dispersions of liquid phase exfoliated materials, where the amounts can be relatively low. As masses on the milligram scale are already enough for this approach, freeze-drying of 2DM dispersions typically yields sufficient material. It should be highlighted that this drying method both removes water as a potential background signal (vide supra) and avoids degradation of the 2D material[27].

Potassium bromide (KBr) is a standard matrix material for mid-infrared spectroscopy. However, below 400 cm^{-1} polyethylene (PE) powder is commonly suggested, as it is transparent the far-infrared.[28] The mid-infrared bands of PE however limit its usability in the MIR, as it has intense bands intrisically. In the case where bands both in the mid- and far-infrared are of scientific interest a common compromise is the use of CsI, due to its lower reported cut-off ($\sim$ 192 cm^{-1})[28] in the far infrared compared to KBr. Nonetheless all matrix materials should be analyzed before use, as commercial powders may often contain residues leading to spectral artifacts. Both PE (ThermoFisher A10239.22) and CsI (ThermoFisher 10022) powders were analyzed in Fig. 4, showing the expected MIR bands for PE, while also demonstrating that commercial CsI also exhibits a few distinct bands in the MIR that need to be noted to avoid misinterpreting them as analyte bands- However, they are weaker by roughly a factor of 8. As the same powder is typically used for background measurements, most of the powder related bands are minimized upon adding the analyte, however some of the CsI related bands remain in the spectrum

(highlighted in grey boxes in Fig. 3). For clarity it should be stressed that the observed bands in the CsI spectrum are not attributed to CsI itself but impurities in the commercial powder or potential reaction products due to atmospheric water. Having established data evaluation, setup and choice of matrix material the final step for a successful DRIFT measurement is to achieve an adequate mixing ratio of matrix and analyte material.

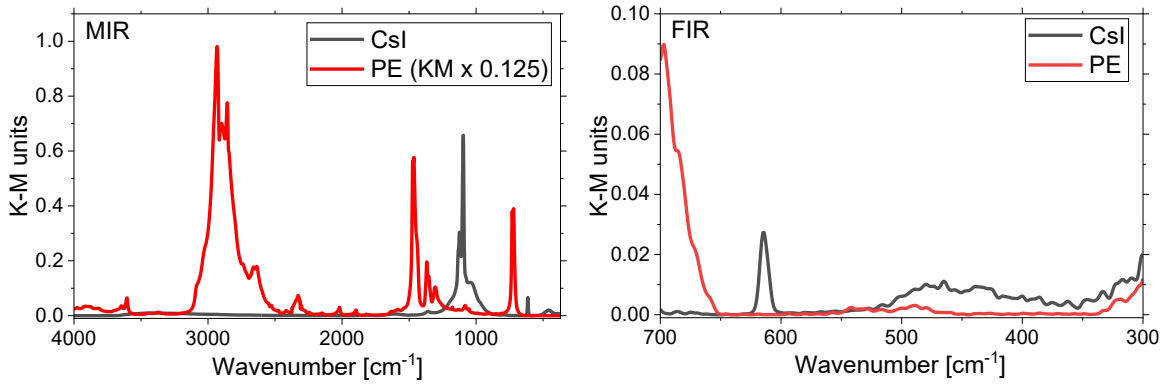

Figure 4: MIR & FIR Spectra of pure CsI and PE powders. *Note that to have a common background an abrasive aluminum pad was used for background measurement. KM units of PE in the MIR were reduced by a factor of 8 to allow for simultaneous visualization of CsI.*

For highly absorbing analytes, spectral transmission values close to 0 % can be observed during measurements, clearly highlighting the necessity to find appropriate dilution in the matris. In the case of common organic samples, dilution factors between 10-20× were reported to give reasonable spectra[29]. From experience working with MoS_2-based samples, a dilution factor of ~ 100× of analyte and matrix material is necessary to achieve reliable spectra. To demonstrate this, we prepared a small series of different powder dilutions from a freeze-dried LPE MoS_2 dispersion with CsI and measured their spectra (Fig. 5). The mode around 467 cm^{-1} which represents the out-of-plane MoS_2 can no longer be distinguished from instrument noise at dilutions higher than 100× which justifies this minimum MoS_2 amount requirement.

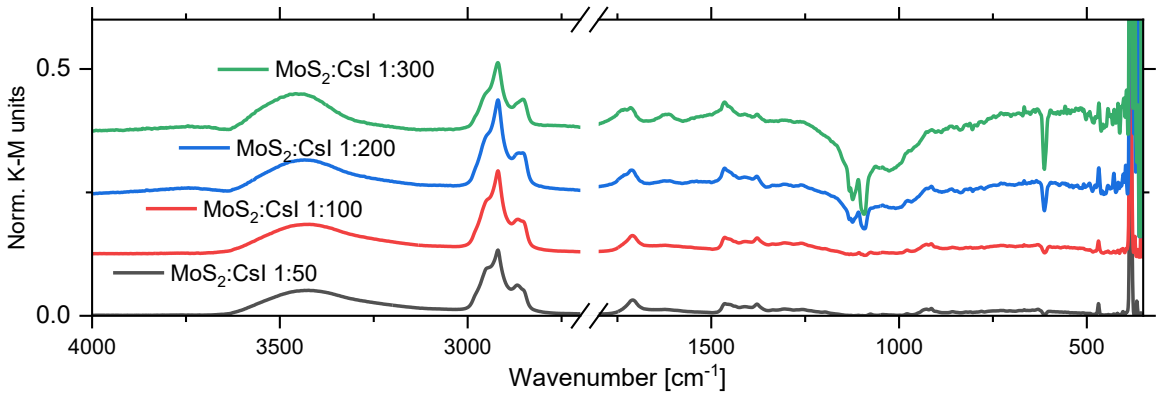

Figure 5: DRIFT spectra in the MIR of liquid phase exfoliated MoS_2. *Measurements of LPE MoS_2 ($\langle N \rangle_{vf}$ = 9) in different dilutions in CsI matrix. Dilutions are given in mass ratios. Spectra were normalized to the in plane Mo-S mode and offset for clarity.*

To demonstrate the applicability of this approach to non-2D materials and also highlight the comparability of this approach to transmission or ATR based experiments, common surfactants utilized in liquid phase exfoliation were analyzed (Fig. 6) and show excellent agreement with data shown in online databases[30]. This points to the potential application of this method to probe organic residues on 2D material surfaces. Within 2D-PRINTABLE, we have applied it to track organic residues on the 2DM surface for different additives and exfoliation conditions and also were able to apply it to gain deeper insights into the binding motif for (covalently) functionalized nanosheets, as already reported in Deliverable D2.1. A publication dedicated to DRIFT to elaborate purification protocols is currently in peer review.

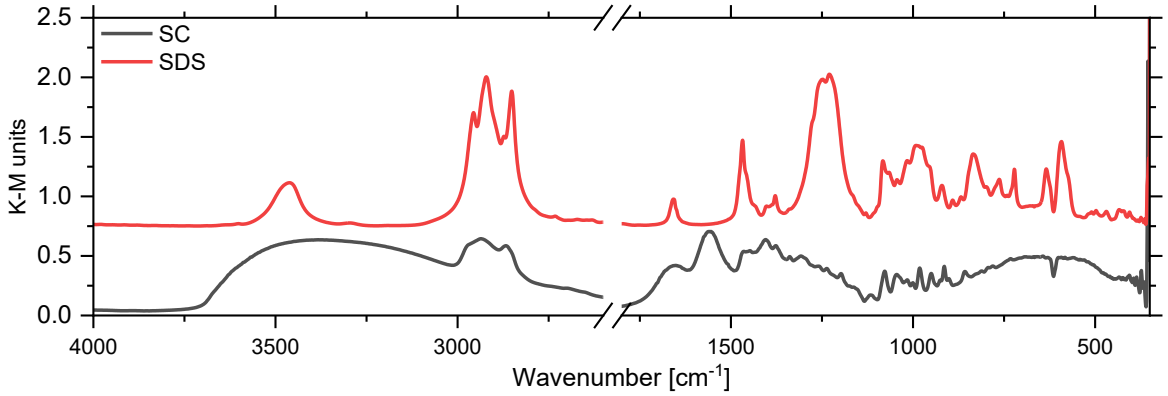

Figure 6: MIR-DRIFT spectra of common surfactants used in liquid-phase exfoliation. *Spectra for sodium cholate (SC) and sodium dodecyl Sulfate (SDS) (Sigma Aldrich C1254-100g; L3771-100g) in CsI matrix. Spectra were offset for clarity.*

3.1.2 FIB-SEM Nanotomography

While protocols to utilise DRIFT spectroscopy have been developed to characterise additives and contaminants on nanosheet surfaces as part of D4.3, the FIB-SEM nanotomography technique has been optimised to quantify the morphology of the 2DM networks/devices they make up. As described in Section 2.2.1, this process involves preparing and imaging hundreds of sequential cross-sections of 2DM networks and their devices using a dual-beam FIB-SEM microscope. The resolution conferred by this technique (voxel size of $\sim 5 \times 5 \times 15$ nm) offers unprecedented insights into the nanostructure of these films and has opened a rich parameter space for quantitative morphological analysis. Briefly, once a stack of high-resolution network cross-sections have been imaged in the SEM, these images are classified into their discrete phases (i.e. nanosheets or pores) using trainable machine learning[5,30]. The result of this process is a set of binarised image stacks with each only containing information only a single phase (i.e. pores or nanosheets). These stacks are then aligned and interpolated using Dragonfly to reconstruct each phase in 3D, such as the nanosheet network or the pore volume. Crucially, this facilitates quantitative analysis of each phase with nanometre-resolution, while also allowing the interfaces between these phases to be characterised. The details of this process are described in detail in Section 2.2.1, as well as several papers published as part of the work undertaken in D4.3[1-3]. The protocols presented here build upon initial work undertaken as part of D4.1.

3D reconstructions of printed LPE and EE graphene networks deposited under identical conditions are shown in Fig. 7a, while their corresponding pore volumes are shown in Fig. 7b. The simplest measurement that can be made on such 3D images is to determine the free space inside the network,

known as the porosity, P_{Net}. This is performed by counting all the voxels labelled as pores in the 3D image and dividing it by the total number of voxels in the image labelled as pores or nanosheets, as is routinely done in both FIJI and the Taufactor application in MATLAB[30]. For example, the LPE graphene network shown in Fig. 7a has a porosity of 43%, while the EE graphene network (Fig. 7b) is much more conformally tiled resulting in a value of P_{Net} = 2%.

Protocols to measure the connectivity of both the pore and nanosheet volumes in each direction through the network have also been developed by calculating their tortuosity factors, κ_{Net}, using the Taufactor application in MATLAB. Here, a reduction in the diffusive flux through the network in the *x*-, *y*- and *z*-directions is measured due to convolutions the in the network structure. For example, a value of κ_{Net} = 1 for a nanosheet network implies a perfectly connected film, with unimpeded paths directly through the volume. If there are pores (or other phases) within the nanosheet network, the path through the volume becomes more complex, leading to values of κ_{Net} > 1. Thus, by measuring κ for the nanosheet or pore volumes, it provides a quantitative metric for how well-connected or continuous each phase is. While the LPE graphene network (Fig. 7a) is qualitatively much more porous and disordered than its EE counterpart (Fig. 7b), the measured κ_{Net} -values suggest the EE film is extremely well connected with a value of κ_{Net} = 1.05 (approaching the limit of a perfect monolithic volume). The increased disorder in LPE film is reflected by a value of κ_{Net} = 1.38, in line with literature values for printed LPE graphene films[31]. This allows changes in the network porosity and connectivity, which are highly relevant to forming networks with improved interflake contacts (as discussed in D5.2), to be linked to nanosheet type or aspect ratio and can inform device fabrication protocols[1]. Similarly, protocols to measure the specific surface area, pore shape and size nanosheet restacking in printed 2DMs have been established.

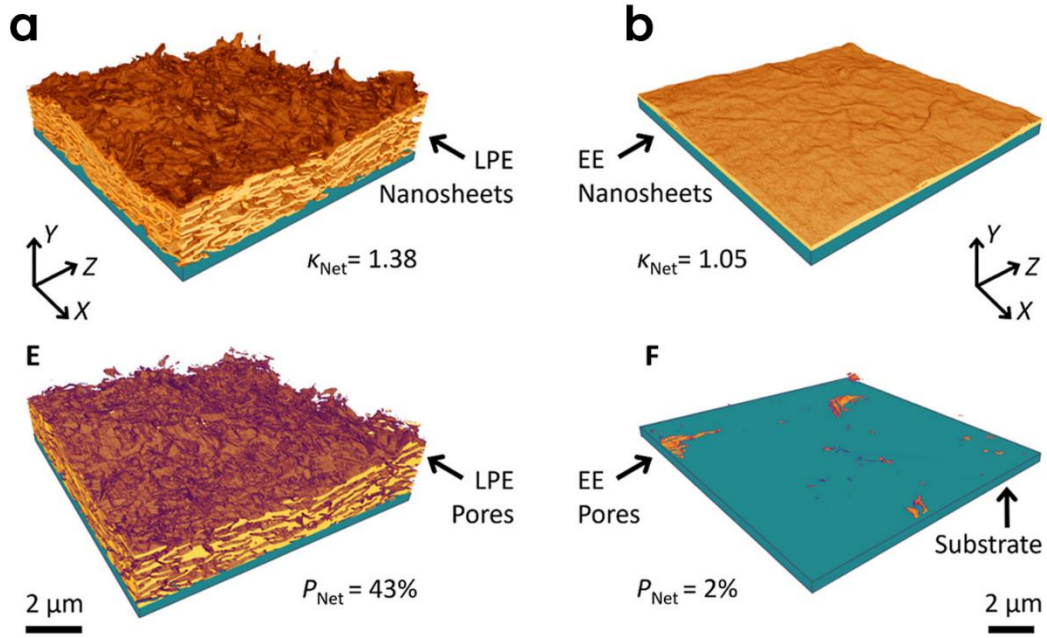

Figure 7: Printed LPE & EE graphene network morphology. *3D reconstructions of the nanosheet and pore volumes for the LPE* ***(a)*** *and EE* ***(b)*** *graphene networks generated using FIB-SEM nanotomography. The network porosity, P_{Net}, and in-plane tortuosity factor, κ_{Net}, is given for both networks.*

As part of D4.3, protocols to quantify the alignment and orientation in printed 2DM networks have been developed. By applying a 3D distance transform watershed algorithm to the 3D image of the

printed LPE graphene network (Fig. 7a) in FIJI[6,8], the contiguous nanosheet network can be broken down into individual nanosheets. By then modelling each nanosheet as an equivalent ellipsoid (Fig. 8a) and finding its eigenvectors, the nanosheet orientation can be determined. Here, the eigenvector describing the smallest axis of each ellipsoid is in the same direction as the normal vector of the nanosheet, $\hat{n}$ (Fig. 8a, inset). By then measuring the polar angle between $\hat{n}$ and the *Y*-axis (out-of-plane direction, perpendicular to the substrate), the angle describing the nanosheet orientation, ϕ_{NS}, can be measured for each nanosheet in the network. Where $\phi_{NS} = 0°$, the nanosheet is lying perfectly flat in the plane of the film, while values of $\phi_{NS} > 0°$ suggest that there is disorder in the nanosheet stacking within the network. A histogram of measured ϕ_{NS} values for the LPE graphene network is shown in Fig. 8b. Here, we see a broad distribution of nanosheet orientations, reflective of the disorder visible in the 3D image in Fig. 7a, with a mean value of $\phi_{NS} = 13.6°$.

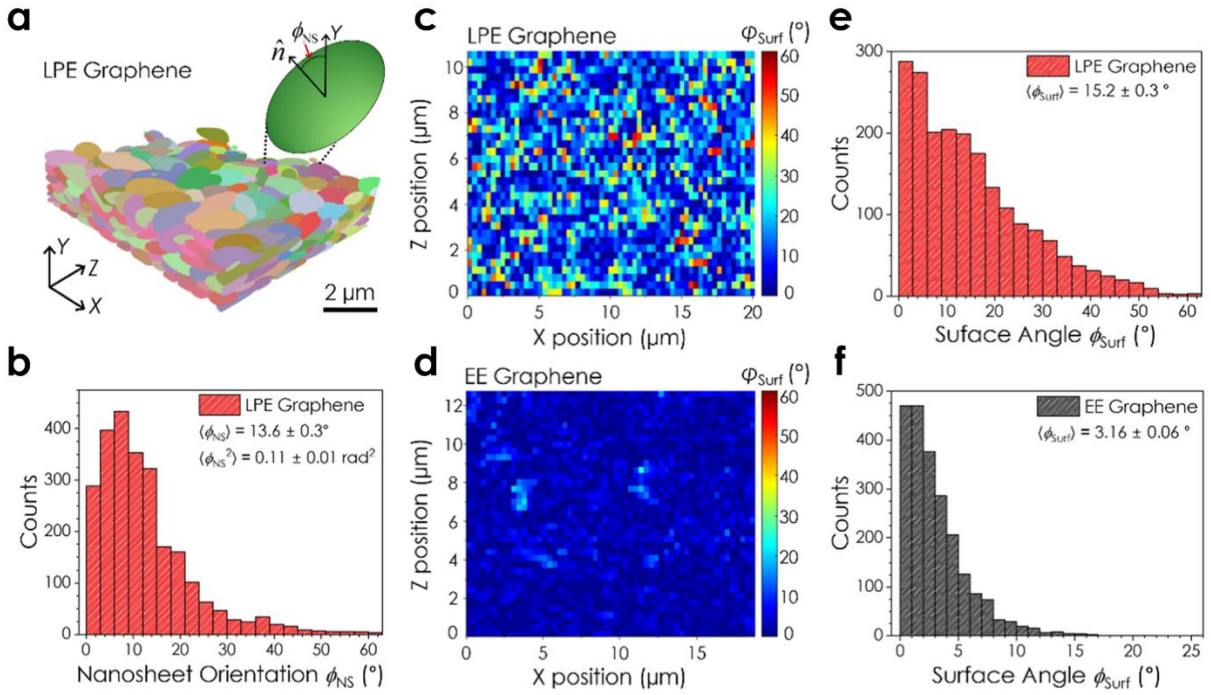

Figure 8: Nanosheet orientation and network surface analysis. (a) *Reconstruction of a portion of a LPE graphene network where discrete nanoplatelets have been replaced with equivalent ellipsoids for orientation analysis. Inset: schematic of an ellipsoid, showing the angle, ϕ_{NS}, between a nanosheet normal vector, $\hat{n}$, and the out-of-plane Y-direction (n = 2538 nanosheets).* ***(b)*** *Histogram of ϕ_{NS} values for each of the nanosheets in the LPE graphene network shown in* ***(a)****.* ***(c-d)*** *Surface gradient maps for the LPE* ***(c)*** *and EE* ***(d)*** *graphene networks. The network surfaces were split into discrete tiles and the angle between the normal vector describing each surface tile and the out-of-plane Y-direction is given by ϕ_{Surf}.* ***(e-f)*** *Histograms of ϕ_{Surf} values for the LPE* ***(e)*** *and EE* ***(f)*** *graphene networks. The average surface angles for the LPE and EE graphene networks were found to be $<\phi_{Surf}>$ = 15.2 ± 0.3° (n = 2016) and $<\phi_{Surf}>$ = 3.16 ± 0.06° (n = 2226), respectively.*

While the orientation of nanosheets within the network can influence the network structure and charge transport, it is the alignment of nanosheets at the network surface that is most relevant to interfacial quality in printed vertical heterostacks and devices. This is highly relevant to the work in

D3.3: Printed heterostructure fabrication. In simplest terms, this can be determined by measuring the root-mean-square roughness, S_q, of the top surface of a 2DM network reconstructed using FIB-SEM NT. Here, values of S_q = 24 ± 1 nm and S_q = 126 ± 3 nm were found for the printed EE and LPE graphene networks shown in Fig. 7a-b respectively. The comparatively smaller S_q for the network of EE graphene nanosheets is consistent with more well-aligned nanosheets and a more smooth and continuous network surface. We can quantitatively measure this alignment using surface gradient maps of the EE and LPE graphene networks (Fig. 8c-d). Here, the top surface of each network volume was split into grids of equally sized tiles (330 × 330 nm) for orientation analysis. By approximating each surface tile as a 2D plane using least squares fitting in MATLAB[1], the polar angle between its normal vector and the *Y*-axis could once again be found. We denote this angle as ϕ_{Surf}. A surface tile where ϕ_{Surf} = 0° has a normal vector parallel to the out-of-plane *Y*-direction, meaning the surface is perfectly flat. The surface gradient maps in Fig. 8c-d share a common colour bar scale for ϕ_{Surf} and show the LPE graphene network surface to be significantly more disordered. The degree of this disorder can be quantified by plotting histograms of ϕ_{Surf} for each tile in the LPE and EE graphene networks (Fig. 8e-f). The LPE graphene network in Fig. 8e exhibits a broad distribution of ϕ_{Surf} values that span a range of 0 – 61 °, with a mean value of $\phi_{\mathrm{Surf,\,LPE}}$ = 15.2 ± 0.3°. In contrast the EE graphene network (Fig. 8f) exhibits a much narrower distribution with a mean value of $\phi_{\mathrm{Surf,\,EE}}$ = 3.2 ± 0.1°. Such protocols provide quantitative measurements of the nanosheet alignment at the surfaces of both these networks and gives numerical outputs via ϕ_{Surf}. In this case, these can be used to show how networks of printed EE nanosheets provide more well-aligned, smoother and more homogeneous interfaces than their LPE counterparts. This can be used to benchmark interfacial quality in printed 2DM networks going forward.

3.2 Contribution to project (linked) Objectives

Protocols for new characterisation methodologies that assess both nanosheet cleanliness and 2DM network/device structure have been developed. The results of D4.3 offer a roadmap towards producing cleaner nanosheets with improved interflake contacts and functionalisation potential, while also offering a means to characterise the structure and interfaces within the networks and devices they make up. This represents a significant contribution to the overall objectives of 2D-PRINTABLE. More specifically, the work presented in D4.3 contributes towards O4.1: Basic characterization of as-exfoliated and functionalized nanosheet building blocks, O4.2: Establish basic and advanced characterization of nanosheet networks and heterostructures to assess morphology and nanosheet coupling and O4.3: Develop new methodologies to characterize exfoliated nanosheets, in particular new materials and networks. In addition, the results from D4.3 will inform work towards achieving O6.1: TFTs with charge carrier mobilities for both *p*- and *n*-type exceeding 100 $cm^2(Vs)^{-1}$ and O6.2: First demonstration of operational all-printed, all-nanosheet PV cells (PCE>10%) and LEDs (EQE>10%).

3.3 Contribution to major project exploitable result

N/A

4 Conclusion and Recommendation

In summary, Deliverable 4.3 has developed characterisation protocols for DRIFT spectroscopy and FIB-SEM nanotomography, providing complementary methodologies to address nanosheet cleanliness and network morphology in printed 2DM systems. For DRIFT spectroscopy, procedures were established using LPE MoS_2 nanosheets as a model system. These protocols allow for the detection of organic residues and additives across mid- and far-infrared ranges, providing a sensitive means of assessing nanosheet cleanliness following exfoliation and processing. By identifying residues that increase R_J and inhibit further functionalisation, this methodology can inform additional cleaning steps and ensure that the produced nanosheets can be both electrically optimised and chemically accessible for integration into heterostructures. For FIB-SEM NT, protocols for three-dimensional reconstruction and quantitative analysis of printed 2DM networks were advanced. This technique has been applied to a host of 2DM networks and devices, but here EE and LPE graphene networks were used as model systems. Clear morphological differences were observed between LPE and EE graphene films, with EE networks exhibiting lower porosity and improved connectivity, consistent with their enhanced charge transport properties. These outcomes, published in peer-reviewed works acknowledging 2D-PRINTABLE[1-3], demonstrate the impact of this methodology, with further technique developments underway.

Together, the two protocols establish a dual strategy: DRIFT spectroscopy can be used to inform the production of cleaner, functional nanosheets free from detrimental residues, while FIB-SEM NT benchmarks and guides the optimisation of network morphologies. Embedding these protocols within the 2D-PRINTABLE workflow provides a reproducible route to printed devices with improved interfaces, tuneable chemistries, and enhanced transport properties.

5 Risks and interconnections

5.1 Risks/problems encountered

N/A

5.2 Interconnections with other deliverables

Deliverable 4.3 is linked with several other deliverables within 2D PRINTABLE. It builds upon the work presented in D2.1: Tuneable functionalization of TMDs, D3.1: Ink production & printing and D4.1: Characterisation of nanosheets, networks and heterostacks built from initially available 2D materials. Furthermore, the results of D4.3 will contribute to future deliverables including D4.4: Characterisation of networks and heterostructures, D6.1: Beyond-state-of-the-art all-nanosheet TFTs, and D6.2: All-printed, all-nanosheet diodes-type devices.

6 Deviations from Annex 1

N/A

7 References

1 Caffrey, E. *et al.* Quantifying the Influence of Nanosheet Aspect Ratio on Network Morphology and Junction Resistance in Solution-Processed Nanosheet Networks. *ACS Nano* **19**, 33118-33133, doi:10.1021/acsnano.5c04008 (2025).

2 Coleman, E. *et al.* Extracting the Temperature Dependence of Both Nanowire Resistivity and Junction Resistance from Electrical Measurements on Printed Silver Nanowire Networks. *ACS Applied Electronic Materials* **7**, 806-815, doi:10.1021/acsaelm.4c01965 (2025).

3 Gambini, L. *et al.* Video frame interpolation neural network for 3D tomography across different length scales. *Nature Communications* **15**, doi:10.1038/s41467-024-52260-2 (2024).

4 Ott, S. *et al.* Impact of the MoS2 Starting Material on the Dispersion Quality and Quantity after Liquid Phase Exfoliation. *Chemistry of Materials* **31**, 8424-8431, doi:10.1021/acs.chemmater.9b02336 (2019).

5 Arganda-Carreras, I. *et al.* Trainable Weka Segmentation: a machine learning tool for microscopy pixel classification. *Bioinformatics* **33**, 2424-2426, doi:10.1093/bioinformatics/btx180 (2017).

6 Schindelin, J. *et al.* Fiji: an open-source platform for biological-image analysis. *Nature Methods* **9**, 676-682, doi:10.1038/nmeth.2019 (2012).

7 Cooper, S. J., Bertei, A., Shearing, P. R., Kilner, J. A. & Brandon, N. P. TauFactor: An open-source application for calculating tortuosity factors from tomographic data. *SoftwareX* **5**, 203-210, doi:10.1016/j.softx.2016.09.002 (2016).

8 Legland, D., Arganda-Carreras, I. & Andrey, P. MorphoLibJ: integrated library and plugins for mathematical morphology with ImageJ. *Bioinformatics*, doi:10.1093/bioinformatics/btw413 (2016).

9 Song, O. & Kang, J. Solution-Processed 2D Materials for Electronic Applications. *ACS Applied Electronic Materials* **5**, 1335-1346, doi:10.1021/acsaelm.2c01784 (2023).

10 Kiriya, D., Tosun, M., Zhao, P., Kang, J. S. & Javey, A. Air-Stable Surface Charge Transfer Doping of MoS2 by Benzyl Viologen. *Journal of the American Chemical Society* **136**, 7853-7856, doi:10.1021/ja5033327 (2014).

11 Yang, L. *et al.* Chloride Molecular Doping Technique on 2D Materials: WS2 and MoS2. *Nano Letters* **14**, 6275-6280, doi:10.1021/nl502603d (2014).

12 Backes, C. *et al.* Edge and confinement effects allow in situ measurement of size and thickness of liquid-exfoliated nanosheets. *Nature Communications* **5**, doi:10.1038/ncomms5576 (2014).

13 Mack, E. A. *et al.* Morphological and Electronic Control of Interfacial Charge Transfer in 2D Transition Metal Dichalcogenide Hybrids. *ACS Nano* **19**, 28576-28587, doi:10.1021/acsnano.5c07850 (2025).

14 Mak, K. F. *et al.* Tightly bound trions in monolayer MoS2. *Nat Mater* **12**, 207-211, doi:10.1038/nmat3505 (2013).

15 Saito, R., Tatsumi, Y., Huang, S., Ling, X. & Dresselhaus, M. S. Raman spectroscopy of transition metal dichalcogenides. *Journal of Physics: Condensed Matter* **28**, 353002, doi:10.1088/0953-8984/28/35/353002 (2016).

16 Molina-Sánchez, A., Hummer, K. & Wirtz, L. Vibrational and optical properties of MoS2: From monolayer to bulk. *Surface Science Reports* **70**, 554-586, doi:https://doi.org/10.1016/j.surfrep.2015.10.001 (2015).

17 Hsu, C. *et al.* Thickness-Dependent Refractive Index of 1L, 2L, and 3L MoS_2, $MoSe_2$, WS_2, and WSe_2. *Advanced Optical Materials* **7**, 1900239, doi:https://doi.org/10.1002/adom.201900239 (2019).
18 Vidrine, D. W. in *Handbook of vibrational spectroscopy* (eds J.M. Chalmers & P.R. Griffiths) (John Wiley & Sons, Ltd., 2006).
19 Ramer, G. & Lendl, B. in *Encyclopedia of Analytical Chemistry* (eds R.A. Meyers & R.A. Meyers) (John Wiley & Sons, Ltd., 2013).
20 Kubelka, P. & Munk, F. An article on optics of paint layers. *Z. tech. Phys* **12**, 259-274 (1931).
21 Baulsir, C. F. & Tague, T. J. Technical Note: Introduction to Diffuse Reflectance Infrared Fourier Transform Spectroscopy. (SpectraTech)).
22 Mitchell, M. B. in *Structure-Property Relations in Polymers* Vol. 236 *Advances in Chemistry* Ch. 13, 351-375 (American Chemical Society, 1993).
23 Alcaraz de la Osa, R., Iparragirre, I., Ortiz, D. & Saiz, J. M. The extended Kubelka–Munk theory and its application to spectroscopy. *ChemTexts* **6**, 2, doi:10.1007/s40828-019-0097-0 (2019).
24 Fuller, M. P. & Griffiths, P. R. Infrared Microsampling by Diffuse Reflectance Fourier Transform Spectrometry. *Applied Spectroscopy* **34**, 533-539, doi:10.1366/0003702804731311 (1980).
25 Fuller, M. P. & Griffiths, P. R. Diffuse reflectance measurements by infrared Fourier transform spectrometry. *Analytical Chemistry* **50**, 1906-1910, doi:10.1021/ac50035a045 (1978).
26 Leyden, D. E. & Murthy, R. S. S. Diffuse reflectance Fourier transform IR spectroscopy. *TrAC Trends in Analytical Chemistry* **7**, 164-169, doi:https://doi.org/10.1016/0165-9936(88)85044-1 (1988).
27 Karger, L. *et al.* The Role of Additives in Suppressing the Degradation of Liquid-Exfoliated WS2 Monolayers. *Advanced Materials* **33**, 2102883, doi:https://doi.org/10.1002/adma.202102883 (2021).
28 E-98, A. Standard practice for general techniques for obtaining infrared spectra for qualitative analysis. *ASTM: West Conshohocken, PA, USA* (2021).
29 Monsef Khoshhesab, Z. in *Infrared Spectroscopy - Materials Science, Engineering and Technology* (ed Theophile Theophanides) (IntechOpen, 2012).
30 https://sdbs.db.aist.go.jp/Disclaimer.aspx, visitsed 30.09.2025.
31 Gabbett, C. *et al.* Quantitative analysis of printed nanostructured networks using high-resolution 3D FIB-SEM nanotomography. *Nature Communications* **15**, doi:10.1038/s41467-023-44450-1 (2024).

8 Acknowledgement

The author(s) would like to thank the partners in the project for their valuable comments on previous drafts and for performing the review.

Project partners:

#	Partner short name	Partner Full Name
1	TCD	TCD THE PROVOST, FELLOWS, FOUNDATION SCHOLARS & THE OTHER MEMBERS OF BOARD, OF THE COLLEGE OF THE HOLY & UNDIVIDED TRINITY OF QUEEN ELIZABETH NEAR DUBLIN
2	UNISTRA	UNIVERSITE DE STRASBOURG
3	UKa	UNIVERSITAET KASSEL
4	BED	BEDIMENSIONAL SPA
5	TUD	TECHNISCHE UNIVERSITAET DRESDEN
6	VSCHT	VYSOKA SKOLA CHEMICKO-TECHNOLOGICKA V PRAZE
7	UNR	UNIRESEARCH BV
8	UniBw M	UNIVERSITAET DER BUNDESWEHR MUENCHEN
9	EPFL	ECOLE POLYTECHNIQUE FEDERALE DE LAUSANNE

Disclaimer/ Acknowledgment

This project has received funding from the European Union's Horizon Europe research and innovation programme under grant agreement No 101135196. Views and opinions expressed are however those of the author(s) only and do not necessarily reflect those of the European Union. Neither the European Union nor the granting authority can be held responsible for them.

9 Appendix A - Quality Assurance Review Form

The following questions should be answered by all reviewers (WP Leader, reviewer, Project Coordinator) as part of the Quality Assurance procedure. Questions answered with NO should be motivated. The deliverable author will update the draft based on the comments. When all reviewers have answered all questions with YES, only then can the Deliverable be submitted to the EC.

NOTE: This Quality Assurance form will be removed from Deliverables with dissemination level "Public" before publication.

Question	**WP Leader**	**Reviewer**	**Project Coordinator**
	Claudia Backes (UKa)	Ali Shaygan Nia (TUD)	Jonathan Coleman (TCD))
1. *Do you accept this Deliverable as it is?*	Yes	Yes / No (elaborate)	Yes / No (elaborate)
2. *Is the Deliverable complete?* - *All required chapters?* - *Use of relevant templates?*	Yes	Yes / No (elaborate)	Yes / No (elaborate)
3. *Does the Deliverable correspond to the DoA?* - *All relevant actions preformed and reported?*	Yes	Yes / No (elaborate)	Yes / No (elaborate)
4. *Is the Deliverable in line with the 2D-PRINTABLE objectives?* - *WP objectives* - *Task Objectives*	Yes	Yes / No (elaborate)	Yes / No (elaborate)
5. *Is the technical quality sufficient?* - *Inputs and assumptions correct/clear?* - *Data, calculations, and motivations correct/clear?* - *Outputs and conclusions correct/clear?*	Yes	Yes / No (elaborate)	Yes / No (elaborate)
6. *Is created and potential IP identified and are protection measures in place?*	N/A	Yes / No (elaborate)	Yes / No (elaborate)
7. *Is the Risk Procedure followed and reported?*	N/A	Yes / No (elaborate)	Yes / No (elaborate)
8. *Is the reporting quality sufficient?* - *Clear language* - *Clear argumentation* - *Consistency* - *Structure*	Yes	Yes / No (elaborate)	Yes / No (elaborate)